Morphological Analysis and Differentiation of Benign Cystic Neoplasms of the Pancreas Using Computed Tomography and Magnetic Resonance Imaging

Morphologische Analyse und Differenzierung benigner, zystischer Neoplasien des Pankreas mittels Computertomografie und Magnetresonanztomografie

Authors

C. Grieser[1], G Heine[1], L. Stelter[1], I. G. Steffen[1], J. H. Rothe[1], T. C. Walter[1], C. Fischer[2], M. Bahra[3], T. Denecke[1]

Affiliations

[1] Klinik für Radiologie, Campus Virchow-Klinikum, Charité – Universitätsmedizin Berlin
[2] Medizinische Klinik m. S. Hepatologie und Gastroenterologie, Campus Virchow-Klinikum, Charité – Universitätsmedizin Berlin
[3] Klinik für Allgemein, Viszeral- und Transplantationschirurgie, Campus Virchow-Klinikum, Charité – Universitätsmedizin Berlin

Key words

- MRI
- CT
- cystic pancreatic tumor
- IPMN
- MCN
- SCN

eingereicht 27.6.2012
akzeptiert 11.10.2012

Bibliography

DOI http://dx.doi.org/10.1055/s-0032-1325551
Published online: 29.11.2012
Fortschr Röntgenstr 2013; 185: 219–227 © Georg Thieme Verlag KG Stuttgart · New York · ISSN 1438-9029

Correspondence

Dr. Christian Grieser
Klinik für Strahlenheilkunde, Charité – Universitätsmedizin Berlin Campus Virchow-Klinikum
Augustenburger Platz 1
13353 Berlin
Germany
Tel.: ++ 49/30/4 50 65 74 83
Fax: ++ 49/30/4 50 55 79 01
christian.grieser@charite.de

Zusammenfassung

Ziel: Beurteilung morphologischer Charakteristika und die Etablierung eines standardisierten diagnostischen Algorithmus für die Differenzierung von benignen, zystischen pankreatischen Tumoren (CPTs) mittels Multidetektor-Computertomografie (CT) und Magnetresonanztomografie (MRT) bei Patienten ohne Pankreatitis.

Material und Methoden: Patienten mit histopathologisch gesicherten CPTs und präoperativer Diagnostik mittels MRT und/oder CT, wurden retrospektiv eingeschlossen. Die Bilder wurden durch 3 unabhängige, verblindete, unterschiedlich erfahrene Untersucher bezüglich Morphologie und Kontrastmittelanreicherungen ausgewertet; als Referenz galt der histopathologische Befund. Anhand der erhobenen bildmorphologischen Charakteristika wurde ein standardisierter diagnostischer Algorithmus zur Läsionscharakterisierung entwickelt.

Ergebnisse: Insgesamt wurden 62 Patienten mit insgesamt 64 CPTs (n = 21 intraduktale papilläre muzinöse Neoplasien, n = 10 muzinös-zystische Neoplasien, n = 12 serös-mikrozystische Adenome, n = 3 serös-oligozystische Adenome, n = 6 solide pseudopapilläre Neoplasien, n = 12 neuroendokrine Neoplasien) aus der chirurgischen Datenbank identifiziert. Die gemittelte Gesamtgenauigkeit für alle drei Befunder lag bei 89,9 % für die CT und 93,1 % für die MRT mit steigender Gesamtgenauigkeit längerer Erfahrung des Befunders (jeweils 88,2, 91,5 und 93,8 %; generalisierte Kappa-Wert = 0,69 (CT = 0,64; MRT = 0,76; p < 0,001). Die Genauigkeit des standardisierten diagnostischen Algorithmus lag bei 91,1 %.

Schlussfolgerung: Die Differenzierung benigner CPTs gelingt gut mittels MRT und CT, wobei die MRT der CT überlegen zu sein scheint. Die diagnostische Treffsicherheit ist erfahrungsabhängig. Der standardisierte Algorithmus könnte als Entscheidungshilfe dienen, sollte jedoch noch an einer weiteren Patientenpopulation getestet werden.

Abstract

Purpose: To evaluate morphologic characteristics and establish a standardized diagnostic algorithm to differentiate benign cystic pancreatic tumors (CPTs) in non-pancreatitis patients using multidetector computed tomography (CT) and magnetic resonance imaging (MRI).

Materials and Methods: Patients with histopathologically proven CPTs who had undergone MRI and/or CT and subsequent tumor resection in our institution were retrospectively identified. Images were analyzed for morphology and enhancement patterns by three independent blinded observers. Preoperative image findings were correlated with histopathological results. Based on the evaluated morphologic parameters, a standardized diagnostic algorithm was designed to help characterize the lesions.

Results: A total of 62 consecutive patients with 64 CPTs were identified from the surgical database (21 intraductal papillary mucinous neoplasms; 10 mucinous cystic neoplasms; 12 serous microcystic adenomas; 3 serous oligocystic adenomas; 6 solid pseudopapillary tumors; 12 neuroendocrine neoplasms). The overall averaged accuracy for the 3 observers was 89.9 % for CT and 93.1 % for MRI with increasing overall accuracy in relation to the experience of the observer (88.2 %, 91.5 %, and 93.8 %, respectively). Overall, the generalized kappa value was 0.69 (CT, 0.64; MRI, 0.76); p < 0.001). The accuracy of the standardized diagnostic algorithm was 91.1 %.

Conclusion: It is possible to characterize benign CPTs with MRI and CT, while MRI appears to be superior to CT. Diagnostic accuracy depends on the observer's experience. The standardized algorithm can aid in the differential diagnosis but still needs to be tested in other patient populations.

Introduction

Due to technical improvements and the widespread use of cross-sectional imaging techniques such as magnetic resonance imaging (MRI) and multidetector computed tomography (CT), benign primary cystic pancreatic tumors (CPTs) are being recognized with increasing frequency. The diagnostic and therapeutic management of primarily benign CPTs varies depending on the entity. The most common entities are serous cystic neoplasms (SCNs) (including serous microcystic adenoma [SMA] and serous oligocystic adenoma [SOA]) and mucinous tumors (including mucinous cystic neoplasm [MCN] and intraductal papillary mucinous neoplasm [IPMN]). SCNs are benign and are therefore usually treated conservatively if the patient is asymptomatic. Mucinous tumors may be premalignant and should therefore be treated surgically. Solid pseudopapillary tumors (SPNs) and cystic neuroendocrine neoplasms (NENs) are less common pancreatic tumors that may present as cystic lesions. SPNs predominantly affect young women. They have a low-grade malignant potential with an excellent prognosis after complete resection. The malignant potential of cystic NENs varies substantially and resection has to be considered individually [1]. Because of this variable behavior of primarily benign CPTs, the goal of radiologic imaging is not only the discrimination from malignant tumors but also differentiation between the benign entities [2]. Typical imaging findings are described in the literature for the differentiation of benign CPTs in CT and MRI. However, the differentiation of these lesions based on imaging is still a diagnostic challenge [1 – 11].

Therefore, the purpose of the present study was to retrospectively evaluate CT and MRI findings for the characterization of histopathologically confirmed benign CPTs and to establish a diagnostic algorithm to provide support when making decisions.

Patients and methods

Patients

A total of 62 consecutive patients fulfilling the prerequisites for inclusion (female: 44; male: 18; median age: 55.6; 25th percentile: 45.1 years; 75th percentile: 66.3 years) were identified from the institutional surgical database: digitally archived multidetector CT and/or MRI of the pancreas (at least biphasic contrast-enhanced imaging for both modalities and additionally for MRI unenhanced standard T1- and T2-weighted (T1w, T2w) sequences with and without fat suppression (FS); see below for further details of examination protocols), complete lesion resection with definite histopathological diagnosis of a benign cystic tumor of the pancreas (search period 2001 – 2011). The exclusion criteria were a history or findings of pancreatitis such as pseudocysts and malignant lesions such as (cyst)-adenocarcinoma. The median interval between imaging and surgery was 21 days (25th percentile: 8 days; 75th percentile: 48 days). The institutional review board approved this retrospective study.

Imaging techniques

62 patients with a total of 84 examinations were evaluated (CT: n = 50; MRI: n = 34). Helical CTs were obtained with 4-row (n = 15), 6-row (n = 1), 8-row (n = 11), 16-row (n = 17), and 64-row (n = 6) CT devices according to the institutional standard protocols for abdominal CT and pancreatic imaging, which have evolved over time and differed between scanner types. All examinations were performed with an intravenous contrast agent (injected amount: 100 – 140 mL; iodine concentration: 350 – 400 mg/dL; flow rates: 2 – 4 mL/sec (automatic injection); saline flush: 40 mL) and were bi- or triphasic (bolus tracking was used in 50 % of cases) consisting of an arterial phase (20 – 40-second delay, performed in 80 % of cases), a portal venous phase (40 – 70-second delay, performed in 90 % of cases), and a venous phase (70 – 90-second delay, performed in 60 % of cases). Additional unenhanced scans were acquired in 69 % of cases. The minimal available reconstructed slice thickness varied from 1 to 3.75 mm.

MRI data were obtained with 1.5 T systems (n = 34) using phased-array surface coils. The examination protocols comprised T2w standard 2 D sequences with and without FS and T1w unenhanced 2 D sequences with and without FS. Intravenous application of Gadolinium-based extracellular contrast agents (0.1 – 0.2 mmol/kg body weight according to the manufacturer's recommendation for the different types of contrast agent; manual or automatic injection at approximately 1 – 2 mL/sec flow rate followed by 40 mL saline flush) was followed by at least two contrast phases (2 D or 3 D T1w sequences with FS in accordance with CT; arterial: 50 %; portal venous: 65 %; venous phase: 71 %). MRCP was performed in 27 (79 %) of all examinations with single-shot thick slab and/or 3 D sequences.

Image analysis

A dedicated viewing workstation was used for image analysis (Centricity PACS RA1000, General Electric, Milwaukee, WI). MRI and CT images were reviewed separately in a randomized order blinded to clinical, histopathological, and surgical data by 3 independent observers with 4 (observer 1), 6 (observer 2), and 9 years (observer 3) of abdominal imaging experience. A definitive diagnosis had to be documented for each case by each observer during the blinded read. The histopathological report served as the reference standard.

In a subsequent truth panel read by the observers, descriptional lesion analysis was performed collecting the following parameters: unifocal or multifocal lesion, number of lesions, location, maximum transverse diameter, predominantly solid or cystic or purely cystic, presence and thickness of a cystic wall/capsule and septa, presence of hemorrhage or calcifications, connection to/contact with the pancreatic duct, and contrast enhancement patterns differentiating early enhancement (i. e., highest contrast uptake during the arterial and/or portal venous phase) and late enhancement (i. e., highest uptake during the venous phase).

The truth panel also determined the quality of the scans, which was evaluated with respect to image noise (minor, major, and non-diagnostic) and movement (or other) artifacts (minor, major, and non-diagnostic) affecting at least one examination component decisive for the evaluation of the lesion on a 3-point scale (1: good (minor image noise and moving artifacts); 2: sufficient (at least one major and no non-diagnostic category); 3: poor/non-diagnostic (non-diagnostic image due to noise and/or artifacts)). The quality of contrast-enhanced dynamic imaging was assessed according to predefined criteria of phase-appropriate enhancement: early arterial phase: dominant arterial contrast filling with little pancreatic parenchyma enhancement; portal venous phase: strong portal venous contrast filling with strong pancreatic parenchyma enhancement; venous phase: complete contrast filling of inferior vena cava and liver veins with fading of pancreatic contrast enhancement. The contrast enhancement of the vessels and pancreatic parenchyma in each contrast phase was graded using a 5-point scale: 1: phase-appropriate and strong enhancement; 2: phase-appropriate but weak enhance-

Table 1 Morphologic characteristics of the included lesions.[1]

Tab. 1 Morphologische Charakteristika der eingeschlossenen Läsionen.[2]

	IPMN	MCN	SCN, SMA	SCN, SOA	SPN	NEN
number of pancreatic lesions (%)	21 (32.8)	10 (15.6)	12 (18.8)	3 (4.7)	6 (9.4)	12 (18.7)
pancreatic location						
head	11*	2	8	2	2	4
corpus	3	3	1	–	2	6
tail	3	5	3	1	2	2
total	4	–	–	–	–	–
multifocal	4	–	–	–	–	–
sex						
male	12	–	1	1	–	5
female	9	10*	11	2	6	7
age (years)	63 ± 12*	52 ± 17	59 ± 9	50 ± 17	33 ± 11*	47 ± 11
size (mm)	32 ± 24	57 ± 37	63 ± 45	53 ± 35	48 ± 25	16 ± 8*
structure						
predominantly solid	–	–	–	–	3*	11*
predominantly cystic	3	1	2	–	1*	–
purely cystic	18	9	10	3	2*	1*
microcystic	–*	1	8*	1	–	–
macrocystic	13*	9	4	2	1	1
cystic wall/capsule	10*	9	11	3	–*	1
septa aspect	13*	10	12	1	1	1
contrast uptake						
cystic wall/capsule	9	8	11	3	–	1
septa/solid parts	9	7	12	2	4	1
calcifications	3	3	6	1	2	–
hemorrhage	1	1	1	–	2	–
association/contact with the pancreatic duct	13*	1	1	–	–	–

[1] IPMN: intraductal papillary mucinous neoplasm; MCN: mucinous cystic neoplasm; SCN: serous cystic neoplasm; SMA: serous microcystic adenoma; SOA: serous oligocystic adenoma; SPN: solid pseudopapillary tumor; NEN: neuroendocrine neoplasm; (*), significance level $p < 0.05$ compared to all other lesions.

[2] IPMN = intraduktale papilläre muzinöse Neoplasie; MCN = muzinös-zystische Neoplasie; SCN, serös-zystische Neoplasie; SMA = serös-mikrozystisches Adenom; SOA = serös-oligozystisches Adenom; SPN = solide pseudopapilläre Neoplasie; NEN = neuroendokrine Neoplasie; *Signifikanzlevel $p < 0,05$ im Vergleich zu allen anderen Läsionen.

ment; 3: strong but inappropriate enhancement; 4: inappropriate and insufficient contrast enhancement; 5: missing contrast phase.

Statistics

Statistical analyses were performed using the IBM SPSS software (release 19.0.0.1; SPSS Inc., IBM, Armonk, NY), the R software (version 2.13.2, R Foundation for Statistical Computing, Vienna, Austria) and SAS software (version 9.1.3, SAS Institute Inc., Cary, NC). Diagnostic parameters (sensitivity, specificity, positive predictive value (PPV), negative predictive value (NPV) and accuracy) were calculated using the standard formulas. Sensitivities and specificities were tested according to the method of Bennett [12]. For the analysis of interobserver variability kappa statistics was used (Cohen's and Fleiss kappa coefficient). Due to the small sample size, normality distribution was not assumed and non-parametric tests were consequently performed. The comparison of paired proportions was performed with the McNemar's Chi-squared test with continuity correction. Unpaired proportions were compared using Fisher's exact test. To compare the medians of two groups, we used the Mann-Whitney U-test. Significance was defined by p-values less than 0.05. Concerning the prediction of the different evaluated parameters, a univariate logistic regression model was used. Odds-ratio estimates, confidence intervals and p-values were calculated using the exact logistic regression model provided by the SAS software package.

Results

Image quality

The quality score for CT and MRI was 1 (96 %) or 2 (4 %) and 1 (85 %) or 2 (15 %), respectively. The quality of contrast enhancement for all available contrast phases was rated with a score of 1 in 75 %, 2 in 23 %, 3 in 2 %, and 4 in 0 % of cases for CT (contrast phases missing: 35) and with a score of 1 in 84 %, a score 2 in 10 %, 3 in 6 %, and 4 in 0 % of cases for MRI (contrast phases missing: 39).

Evaluated lesions

In the 62 patients, a total of 64 CPTs were identified and evaluated. The histopathological diagnoses of the CPTs are summarized in **Table 1** (IPMN: adenomas: n = 7 (10.9 %); borderline: n = 14 (21.9 %); main duct: n = 2; branch duct: n = 7; Santorini's duct: n = 1; mixed type: n = 11; MCN: adenomas: n = 7 (10.9 %); borderline: n = 4 (4.7 %); NEN: insulinoma: n = 7 (10.9 %); glucagonoma: n = 2 (3.1 %); non-functional: n = 3 (4.7 %)). All pancreatic lesions were subject to histopathological confirmation.

Morphologic findings

Table 1 shows the evaluated morphologic criteria for the different pancreatic lesions.

IPMNs (**Fig. 1**) were mostly located in the pancreatic head (53 %; $p < 0.05$) in older patients (median: 66 years; only 2 patients were younger than 58 years; $p < 0.05$), with macrocystic appearance (62 %; $p < 0.05$) and contact/association with the pan-

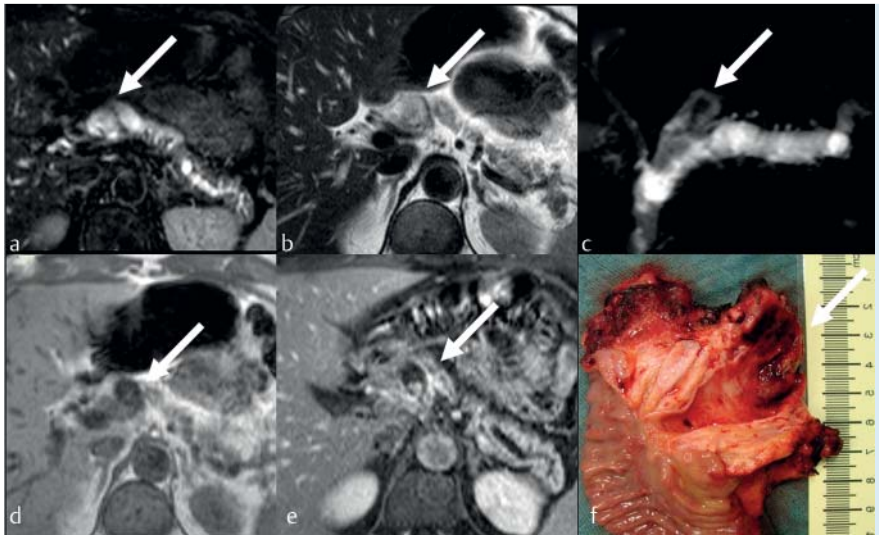

Fig. 1 49-year-old male patient with macrocystic lesion in the pancreatic head (white arrow) with small solid parts and connection to the dilated pancreatic main duct. The resected specimen revealed an intraductal papillary mucinous neoplasm of a branch duct and involvement of the main duct with borderline dysplasia. (MRI: **a** T2-w fat suppressed; **b** T2-w; **c** MRCP; **d** unenhanced T1-w; **e** enhanced [venous phase] T1-w fat suppressed; **f** resected specimen).

Abb. 1 49-jähriger Patient mit makrozystischer Läsion im Bereich des Pankreaskopfes (weißer Pfeil) mit kleinen soliden Anteilen und Anschluss an den erweiterten Pankreashauptgang. Das Resektat zeigte eine intraduktale papilläre muzinöse Neoplasie eines Seitenganges und Übergreifen auf den Hauptgang mit Borderline-Dysplasien. (MRT: **a** T2-w fett gesättigt; **b** T2-w; **c** MRCP; **d** native T1-w; **e** T1-w nach Kontrastmittel [venöse Phase]; **f** Operationspräparat).

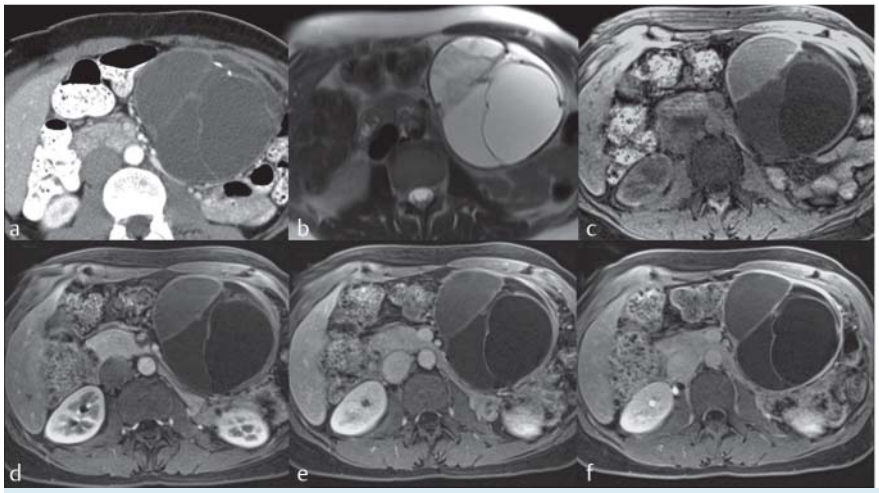

Fig. 2 40-year-old female patient with a large cystic lesion in the pancreatic tail. The lesion presents macrocystic with a marked cystic wall and septae which both show contrast uptake. Furthermore, calcifications and signs of hemorrhage are present. The lesion was histopathologically diagnosed as a mucinous cystic neoplasm (CT: **a** enhanced [arterial phase]; MRI: **b** T2-w; **c** unenhanced T1-w fat suppressed; **d** enhanced T1-w [arterial phase] fat suppressed; **e** enhanced T1-w [portal venous phase]; **f** enhanced [venous phase] T1-w fat suppressed).

Abb. 2 40-jährige Patientin mit makrozystischer Läsion im Pankreasschwanz. Die Läsion zeigt eine deutliche Zystenwand sowie Septae, welche beide Kontrastmittel anreichern; zusätzlich sind Verkalkungen und Zeichen stattgehabter Einblutung vorhanden. Die Läsion wurde histopathologisch als muzinös-zystische Neoplasie diagnostiziert. (CT: **a** früharterielle Phase, MRT: **b** T2-w; **c** native T1-w fett gesättigt; **d** T1-w nach Kontrastmittel [früharterielle Phase], **e** T1-w nach Kontrastmittel [portalvenöse Phase], **f** T1-w nach Kontrastmittel [venöse Phase]).

creatic duct (62 %; $p < 0.05$). A cystic wall/capsule and septae were present in 50 % of cases ($p < 0.05$).

MCNs (**Fig. 2**) were only found in female patients (100 %; $p < 0.05$) without a predominant location ($p > 0.05$). The majority had a purely cystic (90 %; $p > 0.05$) and macrocystic (90 %; $p > 0.05$) presentation with the presence of a cystic wall (90 %; $p > 0.05$) and septae (100 %; $p > 0.05$) with contrast uptake of both in 80 % of cases ($p > 0.05$).

SMAs (**Fig. 3**) were found mostly in female patients (92 %; $p > 0.05$) in the pancreatic head (67 %; $p > 0.05$). A microcystic appearance was found to be significant (67 %; $p < 0.05$). The vast majority of SMAs had a purely cystic presentation (83 %; $p < 0.05$) with the presence of a cystic wall (92 %; $p > 0.05$) and septae (100 %; $p > 0.05$) with contrast uptake (100 %; $p > 0.05$). Furthermore, calcifications were found in 50 % ($p > 0.05$). SOAs (**Fig. 4**) were all purely cystic (100 %; $p > 0.05$) with the presence of a capsule with contrast uptake in 100 % ($p > 0.05$). SPNs (**Fig. 5**) were all found in female patients (100 %; $p > 0.05$) with a mixed appearance of predominantly solid (50 %; $p > 0.05$) and purely cystic (33 %; $p > 0.05$) components without the presence of a cystic wall/capsule (0 %; $p < 0.05$).

NENs (**Fig. 6**) were significantly smaller than all other lesions (16 ± 8 mm; $p < 0.05$) and predominantly solid (92 %; $p < 0.05$).

Univariate logistic linear regression model

Table 2 shows the univariate logistic linear regression model for predictors of different CPTs. For IPMNs, association with the pancreatic duct, a micro- or monocystic appearance and age were found to be predictive factors ($p < 0.05$). For MCNs, a location in the pancreatic corpus or tail and macrocystic appearance were found to be predictive ($p < 0.05$). For SMAs, a microcystic appearance with the presence of calcifications and septal en-

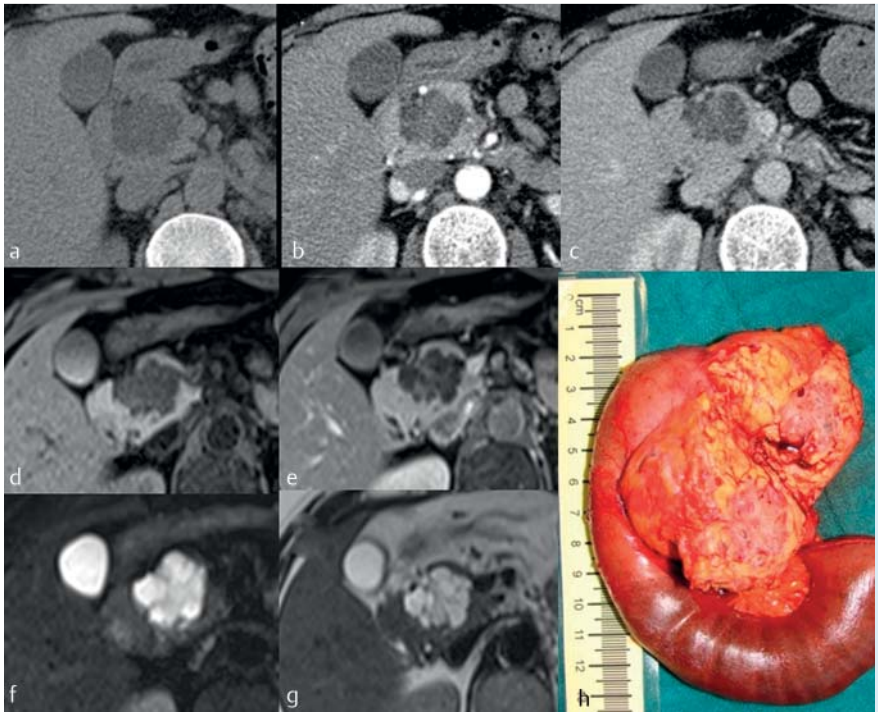

Fig. 3 49-year-old female patient with cystic pancreatic head lesion. Despite the absence of typical calcifications, the lesion shows a microcystic appearance with septal contrast enhancement. The lesion was histopathologically diagnosed as a serous microcystic adenoma (CT: **a** unenhanced; **b** arterial; **c** venous phase; MRI: **d** unenhanced T1-w; **e** enhanced [venous phase] T1-w; **f** T2-w fat suppressed; **g** T2-w; **h**, resected specimen).

Abb. 3 49-jährige Patientin mit zystischer Läsion im Bereich des Pankreaskopfes. Trotz der fehlenden typischen Kalzifikationen zeigt die Läsionen einen mikrozystischen Aufbau mit früharteriellem septalem Enhancement; die Läsion wurde histopathologisch als serös-mikrozystisches Adenom diagnostiziert (CT: **a** native, **b** früharterielle und **c** venöse Phase; MRT: **d** native T1-w, **e** T1-w nach Kontrastmittel [venöse Phase], **f** T2-w fett gesättigt, **g** T2-w, **h** Operationspräparat).

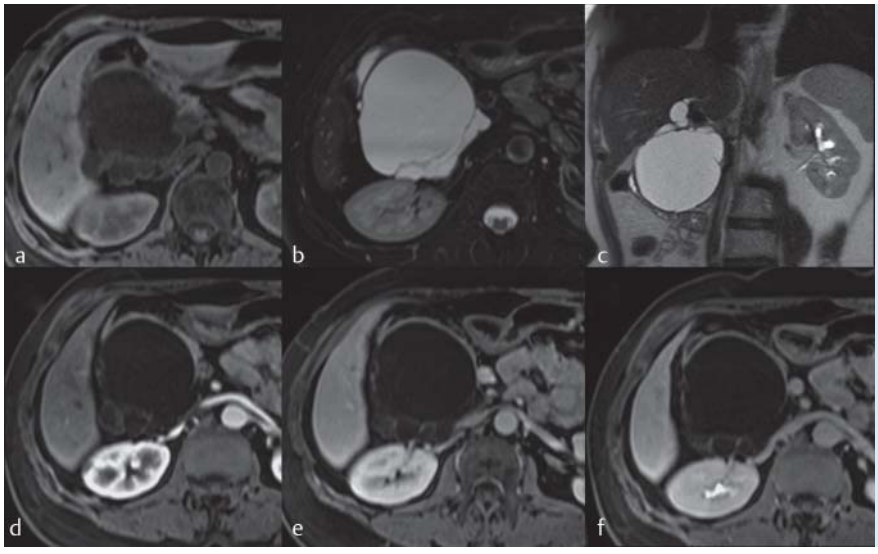

Fig. 4 63-year-old female patient with pancreatic head lesion with macrocystic appearance. The lesion presents with septae which show contrast uptake. The lesion was diagnosed histopathologically as a serous oligocystic adenoma (MRI: **a** unenhanced T1-w fat suppressed; **b** T2-w axial; **c** T2-w coronar; **d** enhanced T1-w [arterial phase] fat suppressed; **e** enhanced T1-w [portal venous phase]; **f** enhanced [venous phase] T1-w fat suppressed).

Abb. 4 63-jährige Patientin mit makrozystischer Läsion im Pankreaskopf. Die Läsion zeigt Septae, die Kontrastmittel anreichern. Die Läsion wurde histopathologisch als serös-oligozystisches Adenom diagnostiziert. (MRT: **a** native T1-w fett gesättigt; **b** axiale T2-w; **c** koronare T2-w; MRT: **d** T1-w nach Kontrastmittel [früharterielle Phase], **e** T1-w nach Kontrastmittel [portalvenöse Phase], **f** T1-w nach Kontrastmittel [venöse Phase].

hancement were found to be predictive ($p < 0.05$). For SPNs, only age was found to be predictive. For NENs, a solid structure and early enhancement were found to be predictive ($p < 0.05$). No predictive factors could be assessed for SOAs due to the small sample size ($n = 3$).

Differential diagnosis by observers and algorithm

Table 3 shows the accuracy and positive predictive values (PPV) of CT and MRI for the differential diagnosis of CPTs by the different observers and the algorithm. For all observers, the overall accuracy of MRI was slightly higher than the accuracy of CT (93.1 % vs. 89.9 %) in the entire patient population. The overall accuracy increased from the least to the most experienced observer (O1 / O2/O3: 88.2 %/91.5 %/93.8 %). The standardized diagnostic algorithm achieved a high overall accuracy of 91.1 % (MRI: 95.1 %; CT: 88.5 %; **Fig. 7**). In the subgroup of the 22 patients who underwent both MRI and CT, the accuracy of MRI was also slightly higher compared to CT (92.4 % vs. 89.6 %). However, this accuracy was not found to be significant for the different observers (observer 1: $p = 0.727$; observer 2: $p = 0.125$; observer 3: $p = 1.0$; all observers: $p = 0.092$) or the standardized diagnostic algorithm ($p = 0.063$).

The interobserver variability of different observers and the algorithm for the differentiation of benign CPTs is shown in **Table 4**. The generalized kappa value was 0.69 for all three observers (CT: 0.64; MRI: 0.76; $p < 0.001$). The generalized kappa value was 0.69 for all three observers and the algorithm (CT studies: 0.64; MRI studies: 0.76; $p < 0.001$).

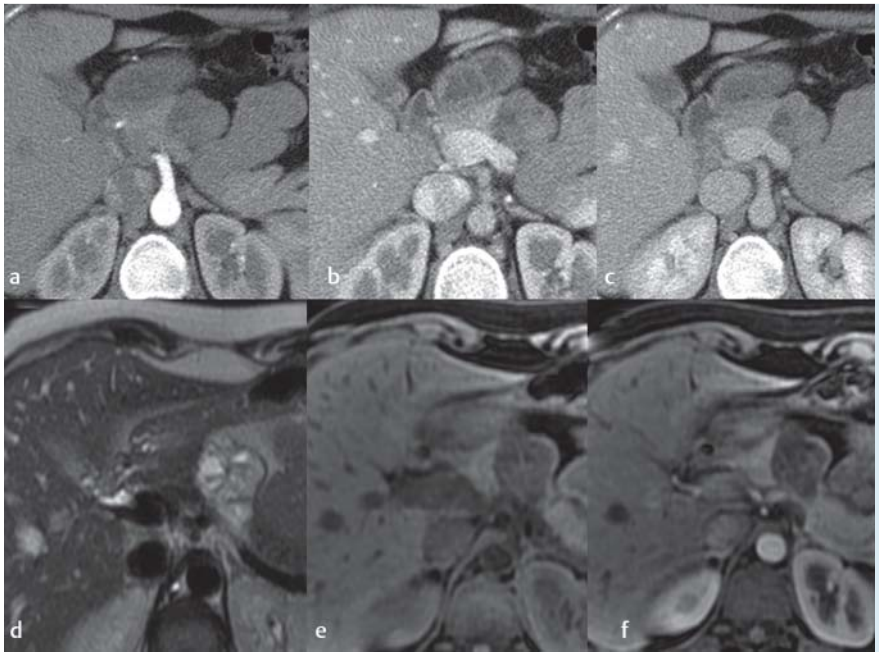

Fig. 5 32-year-old female patient with pancreatic tail lesion. The lesion presents with a mixed appearance of predominantly solid and cystic components with slow accumulation of contrast uptake in the venous phase. The lesion was diagnosed as a solid pseudopapillary tumor (CT: **a** arterial; **b** portal venous; **c** venous phase; MRI: **d** T2-w; **e** unenhanced T1-w; **f** enhanced [venous phase] T1-w).

Abb. 5 32-jährige Patientin mit Läsion im Pankreasschwanz. Die Läsion zeigt ein Nebeneinander von soliden und zystischen Anteilen mit langsamer Kontrastmittelanreicherung in der venösen Phase; die Läsion wurde als solider pseudopapillärer Tumor diagnostiziert (CT: **a** früharterielle, **b** portalvenöse und **c** venöse Phase; MRT: **d** T2-w, **e** native T1-w, **f** T1-w nach Kontrastmittel [venöse Phase]).

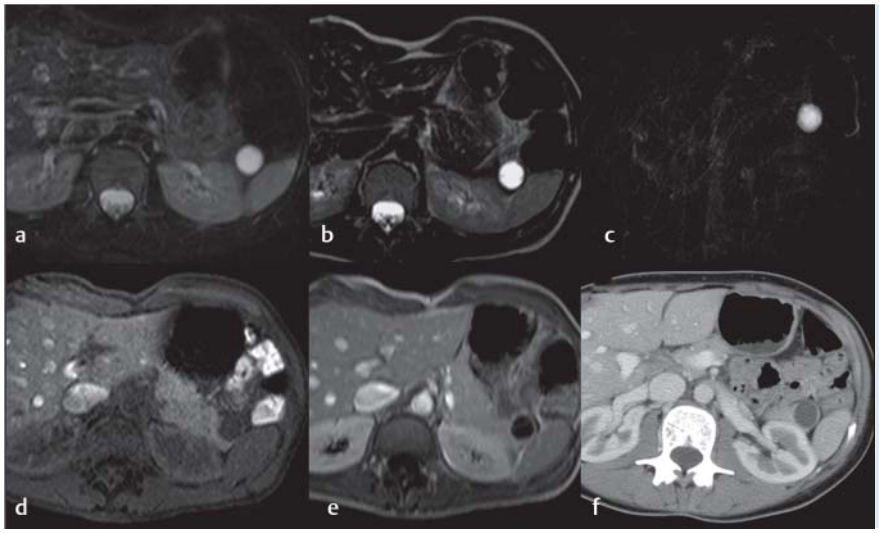

Fig. 6 47-year-old female patient with cystic pancreatic tail lesion. The lesion shows a macro/monocystic appearance with capsular/septal contrast enhancement (arterial phase missing). No contact with the pancreatic duct is present. The lesion was histopathologically diagnosed as a cystic neuroendocrine neoplasm (MRI: **a** T2-w fat suppressed; **b** T2-w; **c** MRCP; **d** unenhanced T1-w; **e** enhanced [venous phase] T1-w fat suppressed; CT: **f** enhanced [venous phase]).

Abb. 6 47-jährige Patientin mit zystischer Läsion im Bereich des Pankreasschwanzes. Die Läsion hat einen makro-/monozystischen Aufbau mit geringer Kapsel/septaler Kontrastmittelanreicherung (arterielle Phase fehlt). Die Läsion wurde histopathologisch als zystische neuroendokrine Neoplasie diagnostiziert (MRT: **a** T2-w fett gesättigt; **b** T2-w; **c** MRCP; **d** native T1-w; **e** T1-w nach Kontrastmittel [venöse Phase]; CT: **f** venöse Phase).

Discussion

In the case of CPTs the challenge of diagnostic imaging with CT and MRI in non-pancreatitis patients is to determine the definitive diagnosis based on the imaging features of a lesion. Several image characteristics are described in the literature for the characterization of benign CPTs on CT and MRI [2 – 5, 7, 13 – 24]. In the present retrospective histopathologically validated study, univariate logistic regression revealed significant characteristics typical for different CPTs such as age, location, association with the pancreatic duct, macro- versus microcystic appearance, presence of calcifications, solid versus cystic structure, and early contrast enhancement, which match the parameters reported in the literature. As in the literature, we also observed overlaps of these criteria between the various (candidate) entities making differential diagnosis challenging.

In the present study, the accuracy of the imaging-based diagnosis of a CPT improved as the years of experience of the radiologist increased, i. e., the overall accuracy improved from the least to the most experienced observer (88.2 %, 91.5 %, and 93.8 %, respectively). According to the generalized kappa value for all three observers (overall kappa: 0.70), the use of MRI (kappa: 0.79) created a higher concordance among readers with different levels of experience than CT (kappa: 0.636). This could be explained by a diagnostic superiority of MRI. However, previous studies showed that CT and MRI have an equal diagnostic accuracy for the characterization of CPTs [22, 25]. Other authors rate MRI as more specific than CT due to a better depiction of septae and cyst contents as well as the pancreatic duct, especially with the use of MRCP [4, 26 – 30]. In the present study, MRI had a slightly better overall accuracy in comparison to CT (93.1 % vs. 89.9 %). As a limitation to this statement it has to be noted that a direct comparison of the performance of MRI and CT examinations was only possible in 22 of the 62 patients. In these patients, neither the overall accuracy (MRI: 92.4 %; CT: 89.6 %) nor the accuracy of single observers or the algorithm was found to be significantly different between the two examination modalities.

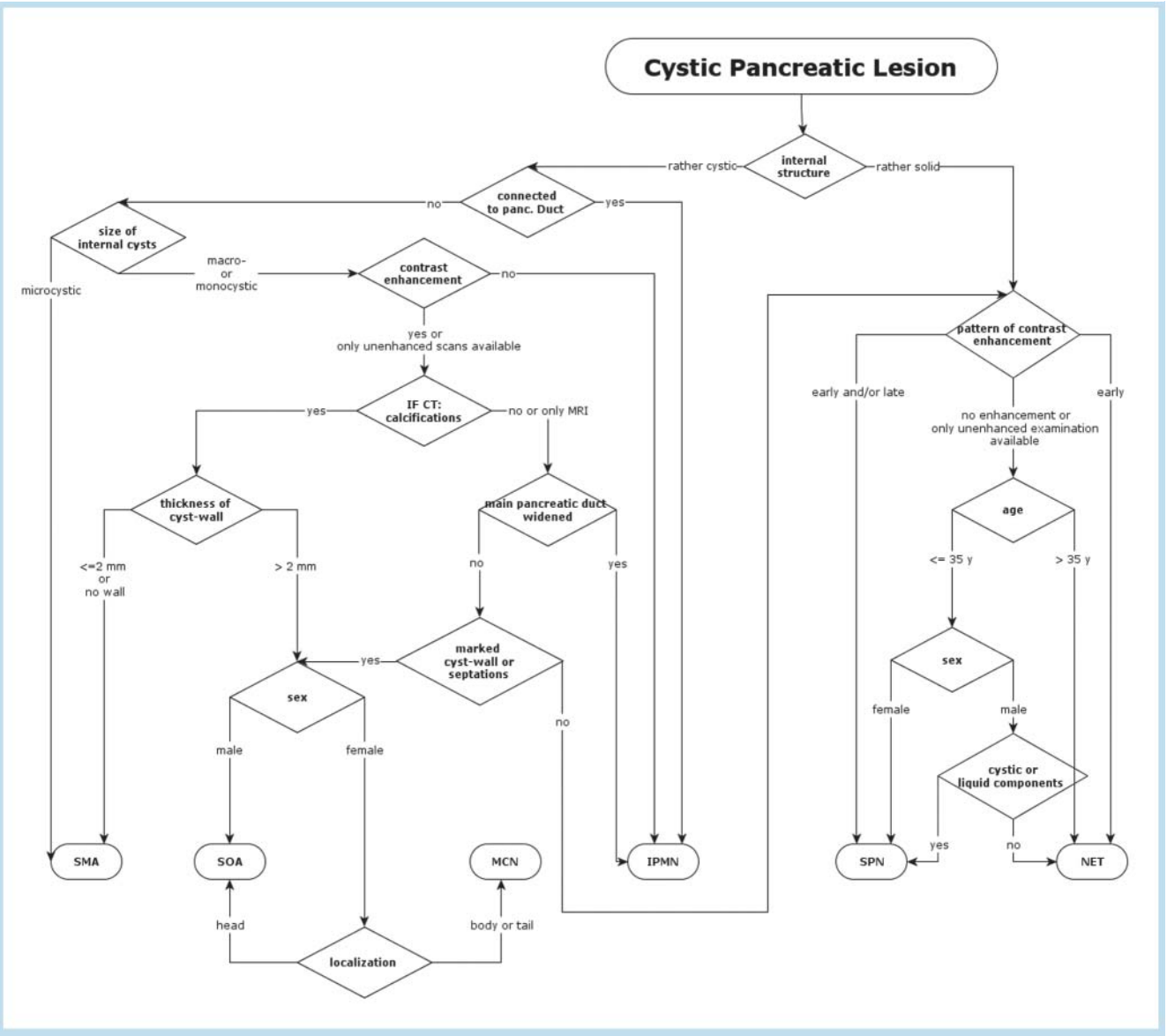

Fig. 7 Diagnostic algorithm for assessing benign pancreatic cystic lesions.

Abb. 7 Diagnostischer Algorithmus zur Beurteilung benigner, zystischer pankreatischer Läsionen.

To lower interobserver variability as a result of different levels of experience, a standardized diagnostic algorithm was developed based on the most significant imaging criteria. This algorithm achieved a good overall accuracy (91.1 %), which was superior to that of the least experienced observer. Thus, it appears to be helpful for inexperienced readers to apply this algorithm to CPTs on CT or MRI in order to increase the accuracy of the differential diagnosis. However, there are some limitations regarding this algorithm. The study population comprised the most frequent but not all of the possible CPT entities in non-pancreatitis patients. The definition of the discriminators used in the algorithm is somewhat subjective and requires training. The algorithm needs to be assessed in a further patient collective with CPTs to evaluate reproducibility. Furthermore, to meet the challenges of the daily routine, the algorithm should be extended to pseudocystic and malignant lesions such as cystadenocarcinomas, which were exclusion criteria in the present study. Moreover, the standardized diagnostic algorithm was developed for a common MRI and CT diagnostic workflow and the accuracy may be improved when separate algorithms optimized for MRI or CT are used. For example regarding MRI, this improvement can be achieved by introducing additional parameters, such as diffusion-weighted imaging, which are not available for CT [31 – 33].

Several limitations to our study have to be mentioned. Due to the retrospective study design and the long examination period (10 years), various MRI and CT scanners and scan protocols with varying contrast phases were used. A distinct quality assessment was performed for all examinations to partly outweigh this drawback revealing at least sufficient image quality regarding image noise, contrast timing, and motion artifacts. Furthermore, most patients were examined in our institution with equivalent examination protocols. Regarding the study population, only patients with histopathologically confirmed cystic benign lesions (IPMNs, MCNs, SCNs, SPNs, and NENs) were included in this study. This was necessary but may have resulted in a selection bias. Also, due to the rare incidence of some of the evaluated CPTs (e. g.,

variable	OR	95 %CI	p-value
IPMN			
age	2.11	1.21 – 4.13	0.005
macrocystic	52.13	4.87–∞	0.000
monocystic	12.02	2.06 – 130.08	0.003
association/contact with the pancreatic duct	29.93	5.34 – 323.41	< 0.001
MCN			
location (corpus or tail)	6.11	1.08 – 64.53	0.038
macrocystic	13.63	1.04 – 2.87	0.006
SMA			
microcystic	2.11	1.21 – 4.13	0.005
calcifications	52.13	4.87–∞	0.000
arterial septal enhancement	12.02	2.05 – 130.08	0.003
SOA	n.a.	n.a.	n.a.
SPN			
age	0.28	0.09 – 0.63	0.000
NEN			
solid structure	29.23	4.87 – 246.96	< 0.001
arterial enhancement	8.14	1.4 – 52.54	0.017

[1] IPMN: intraductal papillary mucinous neoplasm; MCN: mucinous cystic neoplasm; SMA: serous microcystic adenoma; SOA: serous oligocystic adenoma; SPN: solid pseudopapillary tumor; NEN: neuroendocrine neoplasm; n.a.: not assessable.
[2] IPMN = intraduktale papilläre muzinöse Neoplasie; MCN = muzinös-zystische Neoplasie; SMA = serös-mikrozystisches Adenom; SOA = serös-oligozystisches Adenom; SPN = solide pseudopapilläre Neoplasie; NEN = neuroendokrine Neoplasie; n.a., nicht auswertbar.

Table 2 Univariate logistic linear regression model for predictors of different cystic pancreatic tumors (OR: odds ratio; CI: confidence interval).[1]

Tab. 2 Univariate logistische lineare Regressionsanalyse der Prädiktoren für die Differenzierung zystischer pankreatischer Tumore (OR: Odds ratio; CI: Confidence Interval).[2]

Table 3 Accuracy (acc.), and positive predictive values (PPV) of all examinations (all) as well as multidetector computed tomography (CT) and magnetic resonance imaging (MRI) alone for the differentiation of benign cystic pancreatic tumors (CPT).[1]

Tab. 3 Genauigkeit (acc.) und positiv prädiktive Werte (PPV) aller Untersuchungen (all) sowie der Multidetektor-Computertomografie (CT) und der Magnetresonanztomografie (MRT) alleine für die Differenzierung benigner zystischer pankreatischer Tumore (CPT).[2]

	observer 1			observer 2			observer 3			all observers			diagnostic algorithm		
	CT	MRI	All	CT	MRI	All	CT	MRI	All	CT	MRI	All	CT	MRI	All
IPMN															
Acc. (%)	82.7	82.4	82.6	86.5	91.2	88.4	90.4	88.2	89.5	86.5	87.3	86.8	88.5	91.2	89.5
PPV (%)	90.0	71.4	79.2	91.7	84.6	88.0	80.0	75.0	77.8	85.7	76.7	81.2	92.3	84.6	88.5
MCN															
Acc. (%)	80.0	76.5	79.1	80.8	85.3	82.6	88.5	88.2	88.4	83.3	83.3	83.3	90.4	91.2	90.7
PPV (%)	42.9	28.6	38.1	43.8	50.0	45.8	62.5	66.7	63.6	47.4	44.4	46.4	66.7	75.0	69.2
SMA															
Acc. (%)	88.5	91.2	89.5	86.5	94.1	89.5	96.2	100	97.7	90.4	95.1	92.2	84.6	97.1	89.5
PPV (%)	75.0	80.0	76.9	63.6	100	73.3	90.0	100	93.8	75.9	93.3	81.8	58.3	100	70.6
SOA															
Acc. (%)	84.6	97.1	89.5	98.1	97.1	97.7	96.2	97.1	96.5	92.9	97.1	94.6	84.6	94.1	88.4
PPV (%)	0.0	n.a.	0.0	100	n.a.	100	n.a.	n.a.	n.a.	14.3	n.a.	14.3	0.0	33.3	11.1
SPN															
Acc. (%)	96.2	97.1	96.5	96.2	100	97.7	98.1	100	98.8	96.8	99.0	97.7	94.2	100	96.5
PPV (%)	80.0	100	87.5	100	100	100	100	100	100	91.7	100	95.7	100	100	100
NEN															
Acc. (%)	88.5	97.1	91.9	90.4	97.1	93.0	88.5	97.1	91.9	89.1	97.1	92.2	88.5	97.1	91.9
PPV (%)	100	100	100	100	100	100	83.3	100	90.9	93.3	100	96.7	83.3	100	90.9
All CPT															
Acc. (%)	86.9	90.2	88.2	89.7	94.1	91.5	92.9	95.1	93.8	89.9	93.1	91.1	88.5	95.1	91.1
PPV (%)	61.7	70.6	65.4	70.8	82.4	75.6	81.3	85.3	82.9	71.3	79.4	74.7	66.7	85.3	74.4

[1] IPMN: intraductal papillary mucinous neoplasm; MCN: mucinous cystic neoplasm; SMA: serous microcystic adenoma; SOA: serous oligocystic adenoma; SPN: solid pseudopapillary tumor; NEN: neuroendocrine neoplasm; n.a.: not assessable.
[2] IPMN = intraduktale papilläre muzinöse Neoplasie; MCN = muzinös-zystische Neoplasie; SMA = serös-mikrozystisches Adenom; SOA = serös-oligozystisches Adenom; SPN = solide pseudopapilläre Neoplasie; NEN = neuroendokrine Neoplasie; n.a. = nicht auswertbar.

SOAs and SPNs), the statistical conclusions may not be completely relevant (significant).

Conclusion

The characterization of benign CPTs is possible with MRI and CT, with MRI seeming to be superior to CT. The diagnostic accuracy depends on the observer's experience. The standardized algorithm can aid in the differential diagnosis but still needs to be tested in other patient populations.

Table 4 Interobserver variability of different observers and algorithm for the differentiation of benign cystic pancreatic tumors.[1]

Tab. 4 Variabilität zwischen den Befundern und dem Algorithmus für die Differenzierung benigner zystischer pankreatischer Tumore.[2]

observer	CT (kappa)	MRI (kappa)	All (kappa)
O1, O2*	0.69	0.72	0.71
O1, O3*	0.61	0.80	0.68
O2, O3*	0.62	0.76	0.67
O1, O2, O3 +	0.64	0.76	0.69
O1, algorithm*	0.63	0.65	0.65
O2, algorithm*	0.67	0.85	0.74
O3, algorithm*	0.64	0.80	0.71
O1, O2, O3, algorithm+	0.64	0.76	0.69

[1] O: observer; (*): Cohen's kappa coefficient; +: generalized Fleiss kappa coefficient; significance level $p < 0.05$ for all kappa values.

[2] O, Untersucher, *Cohens Kappa Koeffizient, +generalisierter Fleiss Kappa Koeffizient, Singifikanzlevel $p < 0{,}05$ für alle Kappa Werte.

References

1 *Sakorafas GH, Smyrniotis V, Reid-Lombardo KM et al.* Primary pancreatic cystic neoplasms of the pancreas revisited. Part IV: Rare cystic neoplasms. Surg Oncol 2011; 21: 153 – 163
2 *Lopez Hänninen E, Pech M, Ricke J et al.* Magnetic resonance imaging in the assessment of cystic pancreatic lesions: differentiation of benign and malignant lesion status. Acta Radiol 2006; 47: 121 – 129
3 *Buerke B, Heindel W, Wessling J.* Differenzialdiagnose und radiologisches Management von zystischen Tumoren des Pankreas. Fortschr Röntgenstr 2010; 182: 852 – 860
4 *Kalb B, Sarmiento JM, Kooby DA et al.* MR imaging of cystic lesions of the pancreas. Radiographics 2009; 29: 1749 – 1765
5 *Sun HY, Kim SH, Kim MA et al.* CT imaging spectrum of pancreatic serous tumors: based on new pathologic classification. Eur J Radiol 2009; 75: e45 – 55
6 *Yamada Y, Mori H, Hijiya N et al.* Intraductal papillary mucinous neoplasms of the pancreas complicated with intraductal hemorrhage, perforation, and fistula formation: CT and MR imaging findings with pathologic correlation. Abdom Imaging 2011; 37: 100 – 109
7 *Zhang J, Wang PJ, Yuan XD.* Correlation between CT patterns and pathological classification of intraductal papillary mucinous neoplasm. Eur J Radiol 2008; 73: 96 – 101
8 *Mussig K, Bares R, Dudziak K et al.* Multimodale Bildgebung von pankreatischen neuroendokrinen Tumoren. Fortschr Röntgenstr 2008; 180: 373 – 379
9 *Froling V, Denecke T, Pollinger A et al.* Nachweis einer neuroendokrin differenzierten zystischen Pankreasläsion durch die Gallium-68-DOTATOC-PET/CT bei inkonklusiver MRT, CT und Sonografie. Fortschr Röntgenstr 2010; 182: 175 – 177
10 *Lange S, Alzen G, Leder H et al.* Solid-pseudopapillärer Pankreastumor im Kindesalter. Fortschr Röntgenstr 2002; 174: 286 – 290
11 *Krasny A, Pietsch S, Lauenstein T.* Fehldiagnose eines soliden-pseudopapillären Pankreastumors. Fortschr Röntgenstr 2012; 184: 256 – 257
12 *Bennett BM.* On comparisons of sensitivity, specificity and predictive value of a number of diagnostic procedures. Biometrics 1972; 28: 793 – 800
13 *Acar M, Tatli S.* Cystic tumors of the pancreas: a radiological perspective. Diagn Interv Radiol 2011; 17: 143 – 149
14 *Baiocchi GL, Portolani N, Missale G et al.* Intraductal papillary mucinous neoplasm of the pancreas (IPMN): clinico-pathological correlations and surgical indications. World J Surg Oncol 2010; 8: 25
15 *Brugge WR, Lewandrowski K, Lee-Lewandrowski E et al.* Diagnosis of pancreatic cystic neoplasms: a report of the cooperative pancreatic cyst study. Gastroenterology 2004; 126: 1330 – 1336
16 *Chang H, Gong Y, Xu J et al.* Clinical strategy for the management of solid pseudopapillary tumor of the pancreas: aggressive or less? Int J Med Sci 2010; 7: 309 – 313
17 *Fisher WE, Hodges SE, Yagnik V et al.* Accuracy of CT in predicting malignant potential of cystic pancreatic neoplasms. HPB (Oxford) 2008; 10: 483 – 490
18 *Gupta R, Mortele KJ, Tatli S et al.* Pancreatic intraductal papillary mucinous neoplasms: role of CT in predicting pathologic subtypes. Am J Roentgenol Am J Roentgenol 2008; 191: 1458 – 1464
19 *Kawamoto S, Scudiere J, Hruban RH et al.* Solid-pseudopapillary neoplasm of the pancreas: spectrum of findings on multidetector CT. Clin Imaging 2011; 35: 21 – 28
20 *Kim JH, Hong SS, Kim YJ et al.* Intraductal papillary mucinous neoplasm of the pancreas: Differentiate from chronic pancreatits by MR imaging. Eur J Radiol 2012; 81: 671 – 676
21 *Kosmahl M, Pauser U, Anlauf M et al.* Zystische Pankreastumoren und ihre Klassifikation. Pathologe 2005; 26: 22 – 30
22 *Lee HJ, Kim MJ, Choi JY et al.* Relative accuracy of CT and MRI in the differentiation of benign from malignant pancreatic cystic lesions. Clin Radiol 2010; 66: 315 – 321
23 *Morgan DE.* Cystic lesions of the pancreas. Semin Roentgenol 2009; 44: 255 – 265
24 *Rafique A, Freeman S, Carroll N.* A clinical algorithm for the assessment of pancreatic lesions: utilization of 16- and 64-section multidetector CT and endoscopic ultrasound. Clin Radiol 2007; 62: 1142 – 1153
25 *Visser BC, Muthusamy VR, Yeh BM et al.* Diagnostic evaluation of cystic pancreatic lesions. HPB (Oxford) 2008; 10: 63 – 69
26 *Morgan DE, Baron TH, Smith JK et al.* Pancreatic fluid collections prior to intervention: evaluation with MR imaging compared with CT and US. Radiology 1997; 203: 773 – 778
27 *Choi JY, Lee JM, Lee MW et al.* Magnetic resonance pancreatography: comparison of two- and three-dimensional sequences for assessment of intraductal papillary mucinous neoplasm of the pancreas. Eur Radiol 2009; 19: 2163 – 2170
28 *Lopez HanninenE, Amthauer H, Hosten N et al.* Prospective evaluation of pancreatic tumors: accuracy of MR imaging with MR cholangiopancreatography and MR angiography. Radiology 2002; 224: 34 – 41
29 *Waters JA, Schmidt CM, Pinchot JW et al.* CT vs MRCP: optimal classification of IPMN type and extent. J Gastrointest Surg 2008; 12: 101 – 109
30 *Vogl TJ, Zangos S, Eichler K et al.* Radiologische Diagnostik und Intervention von Cholangiokarzinomen (CC). Fortschr Röntgenst 2012; 184: 883 – 892
31 *Wang Y, Miller FH, Chen ZE et al.* Diffusion-weighted MR imaging of solid and cystic lesions of the pancreas. Radiographics 2011; 31: E47 – 64
32 *Sandrasegaran K, Akisik FM, Patel AA et al.* Diffusion-weighted imaging in characterization of cystic pancreatic lesions. Clin Radiol 2011; 66: 808 – 814
33 *Fatima Z, Ichikawa T, Motosugi U et al.* Magnetic resonance diffusion-weighted imaging in the characterization of pancreatic mucinous cystic lesions. Clin Radiol 2011; 66: 108 – 111